INTERNATIONAL JOURNAL FOR NUMERICAL METHODS IN FLUIDS, VOL. 9, 251–262 (1989)

A NEW LOOK AT THEODORSEN'S METHOD IN AEROFOIL THEORY

RAJENDRA K. BERA

Fluid Mechanics Division, National Aeronautical Laboratory, Bangalore 560 017, India

SUMMARY

Theodorsen's method for calculating the incompressible potential flow past an aerofoil is viewed afresh. It is found that some simple modifications to the computational process make the computations relatively faster, easier and more accurate. The new modifications are applicable to the analysis of conventional aerofoils with up to moderate thickness and camber ratios. Several examples are presented to show the effectiveness of the modifications.

KEY WORDS Theodorsen's method Incompressible flow Aerofoil theory Thickness ratio Camber ratio

1. INTRODUCTION

Theodorsen's[1,2] 'exact' but iterative method of calculating the speed (and hence the pressure) distribution on an aerofoil placed in an unbounded uniform ideal fluid flow is a landmark in aerofoil theory. The method is also known to give excellent results for a large class of aerofoils even at the end of the first iteration, a factor important in actual calculations since a solution can then be obtained quickly. Unfortunately, the calculation procedure as reported by Theodorsen or its treatment in textbooks[3–5] leaves the impression that the procedure is cumbersome and further that it may lead to numerical inaccuracies because of several graphical (or numerical) differentiations required in the calculations.

In this paper we shall show that for conventional aerofoils of up to moderate thickness and camber ratios, where an accurate enough solution can be obtained in one or two iterations, the calculation procedure can be performed analytically. The small amount of numerical analysis that must be resorted to when the aerofoil co-ordinates are not given as a Fourier series in the Glauert variable ϕ requires only numerical integration. This new computational strategy makes Theodorsen's method faster, comparatively more accurate and easier to use.

Although viscosity is neglected in ideal fluid flow theory, its results are nevertheless frequently used as the starting point for the further analysis of the corresponding viscous flow. The Theodorsen solution is therefore of primary interest in aerofoil theory.

In the following, Section 2 briefly describes Theodorsen's method, Section 3 contains the new calculation procedure, Section 4 gives examples and Section 5 draws the final conclusions.

2. THEODORSEN'S METHOD

Theodorsen's method is well described in several textbooks,[3–5] hence only a brief description is provided below. The two-step method, based on conformal mapping, maps the aerofoil to a circle

0271–2091/89/030251–12$06.00

Received 24 August 1987
Revised 11 May 1988

(see Figure 1), then relates the flow past a circle to the flow past the aerofoil. The aerofoil C is placed in the z-plane with the aerofoil chord along the x-axis. $\mathbf{V}_\infty$ is the free-stream velocity and α is the aerofoil angle of attack. In the first step, the Joukowski mapping

$$z=\tilde{\zeta}+l^2/\tilde{\zeta}, \qquad l=\text{a real constant} \tag{1}$$

is used to map the aerofoil into a 'pseudo-circle' $\tilde{\mathscr{C}}$ in the $\tilde{\zeta}$-plane. This is best accomplished by locating the critical points $z=\pm 2l$ as follows: near the leading edge, midway between the leading edge and its centre of curvature; and near the trailing edge, midway between the trailing edge and its centre of curvature. (If an edge is sharp or cusped, it becomes a critical point.) However, in practice (and in this paper), one frequently chooses $z=0$ as the aerofoil mid-chord, $z=-2l$ as leading edge and $z=2l$ as trailing edge. For aerofoils of up to moderate thickness and camber ratios, the error is small.

In the second step, the 'pseudo-circle' $\tilde{\mathscr{C}}$ is mapped into a circle $\mathscr{C}$ with centre at $\zeta=0$ in the ζ-plane by an iterated determination of the complex coefficients $C_n=R^n(A_n+iB_n)$, with R as the radius of $\mathscr{C}$, in the mapping function

$$\tilde{\zeta}=\zeta \exp\left(\sum_{n=1}^{\infty} C_n/\zeta^n\right). \tag{2}$$

Let the contours C, $\tilde{\mathscr{C}}$ and $\mathscr{C}$ be described respectively by

$$z=x+iy, \qquad \tilde{\zeta}=l\exp(\psi+i\phi), \qquad \zeta=l\exp(\chi_0+i\theta); \tag{3}$$

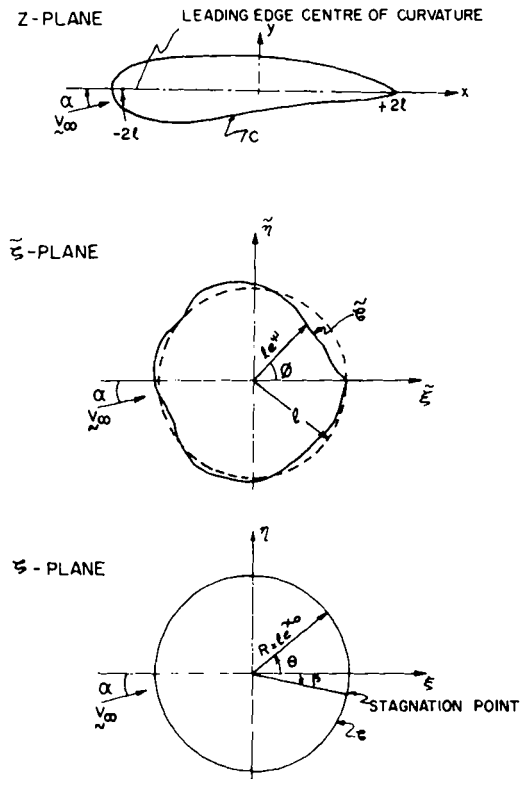

Figure 1. Illustration of Theodorsen's mapping procedure

then

$$\tilde{\zeta} = \zeta \exp\left(\sum_{n=1}^{\infty} C_n/\zeta^n\right) = \zeta \exp\left[(\psi - \chi_0) + \mathrm{i}(\phi - \theta)\right] \tag{4}$$

or

$$\psi - \chi_0 = \sum_{n=1}^{\infty} \left[A_n \cos(n\theta) + B_n \sin(n\theta)\right], \tag{5}$$

$$\varepsilon = \theta - \phi = \sum_{n=1}^{\infty} \left[-B_n \cos(n\theta) + A_n \sin(n\theta)\right], \tag{6}$$

from which we obtain

$$\begin{aligned} \chi_0 &= (1/2\pi) \int_0^{2\pi} \psi(\theta)\, \mathrm{d}\theta, \\ A_n &= (1/\pi) \int_0^{2\pi} \psi(\theta) \cos(n\theta)\, \mathrm{d}\theta, \\ B_n &= (1/\pi) \int_0^{2\pi} \psi(\theta) \sin(n\theta)\, \mathrm{d}\theta \end{aligned} \tag{7}$$

and

$$x = 2l \cosh\psi \cos\phi, \qquad y = 2l \sinh\psi \sin\phi. \tag{8}$$

Also, we have from equations (8)

$$\begin{aligned} \psi = \ln \mathrm{e}^{\psi} &= \ln(\sinh\psi + \cosh\psi) \\ &= \sinh\psi - (1/6)\sinh^3\psi + \ldots \\ &= y/(2l \sin\phi) + \text{third-order terms in aerofoil thickness and camber ratios.} \end{aligned} \tag{9}$$

Note that $l \exp(\mathrm{i}\phi)$ describes a circle in the $\tilde{\zeta}$-plane which maps to a Joukowski aerofoil $\mathrm{C_J}$ in the z-plane. Thus $\exp\psi$ is a measure of the deviation of the aerofoil geometry $\mathscr{C}$ from that of $\mathrm{C_J}$. If the deviations are small, then ψ will be small irrespective of aerofoil thickness and camber ratios. Alternatively, if the aerofoil's thickness and camber ratios are small, ψ will again be small.

The constants χ_0, A_n and B_n are determined by iteration. To begin with, we know ψ as a function of ϕ only from equations (8). In the first iteration we choose $\theta = \phi$ and in subsequent iterations update θ by means of equations (5)–(7) until the desired convergence is reached. In practice, for conventional aerofoils, convergence is rapid. The reason for this will become clear in Section 3.

The speed on the circle $\mathscr{C}$ is given by

$$|\mathscr{W}(\zeta)|_{\mathscr{C}} = 2V_{\infty} |\sin(\alpha + \beta) - \sin(\alpha - \theta)| \tag{10}$$

where $\theta = -\beta$ corresponds to the aerofoil trailing edge where the Kutta condition is applied, and $\mathscr{W}(\zeta)$ is the complex velocity.

The speed on the aerofoil contour C is given by

$$|W(z)|_{\mathrm{C}} = |\mathscr{W}(\zeta)|_{\mathscr{C}} / |\mathrm{d}z/\mathrm{d}\zeta|_{\mathscr{C}} = \frac{V_{\infty}(1 + \mathrm{d}\varepsilon/\mathrm{d}\phi)\,|\sin(\alpha + \beta) - \sin(\alpha - \theta)|\, \mathrm{e}^{\chi_0}}{\sqrt{\{[1 + (\mathrm{d}\psi/\mathrm{d}\phi)^2](\sinh^2\psi + \sin^2\phi)\}}}, \tag{11}$$

where $W(z)$ is the complex velocity and $\phi = 0$ corresponds to the trailing edge. Consequently $\beta = -\varepsilon(\phi = 0)$.

The lift and pitching moment coefficients (Figure 2) are given by

$$C_L = 8\pi(R/c)\sin(\alpha+\beta)$$

$$C_{M_0} = 4\pi(R/c)^2[(B_2+2A_1B_1)\cos(2\alpha) - (A_2+A_1^2-B_1^2)\sin(2\alpha)] \quad \text{about } z=0, \tag{12}$$

$$C_{M_\mu} = C_{M_0} - C_L(m/c)\cos(\delta-\alpha) \quad \text{about an arbitrary point } z=\mu=me^{i\delta},$$

where c is the aerofoil chord length in the z-plane.

3. METHOD OF SOLUTION

Let the aerofoil be described by

$$y(x) = y_c(x) \pm y_t(x), \qquad x_{LE} \leqslant x \leqslant x_{TE}, \tag{13}$$

where $y_t(x)$ and $y_c(x)$ represent the aerofoil semi-thickness and camber distributions respectively. The aerofoil leading edge and trailing edge co-ordinates are $(x_{LE}, 0)$ and $(x_{TE}, 0)$ respectively. In the composite sign $\pm$ the plus refers to the aerofoil upper surface and the minus to the lower surface.

For aerofoils of up to moderate camber and thickness ratios, ψ will be small and we may use the approximations (see equations (8) and (9))

$$\psi \cong y/2l \sin\phi, \tag{14}$$

$$x \cong 2l\cos\phi, \tag{15}$$

$$c \cong 4l. \tag{16}$$

This places the origin of the co-ordinate system in the z-plane at mid-chord and allows the use of the conventional Fourier series expansion for $y(x)$ in the Glauert variable ϕ. Thus

$$y(x) = y(\phi) = (c/2)\sum_{n=1}^{\infty} \hat{a}_n \sin(n\phi) + (c/2)\sum_{m=0}^{\infty} \hat{b}_m \cos(m\phi), \quad 0 \leqslant \phi \leqslant 2\pi, \tag{17}$$

where the real constants $\hat{a}_n$ and $\hat{b}_m$, if not already known, may be found from

$$(c/2)\hat{b}_0 = (1/2\pi)\int_0^{2\pi} y(\phi)\,d\phi,$$

$$(c/2)\hat{b}_m = (1/\pi)\int_0^{2\pi} y(\phi)\cos(m\phi)\,d\phi, \tag{18}$$

$$(c/2)\hat{a}_n = (1/\pi)\int_0^{2\pi} y(\phi)\sin(n\phi)\,d\phi.$$

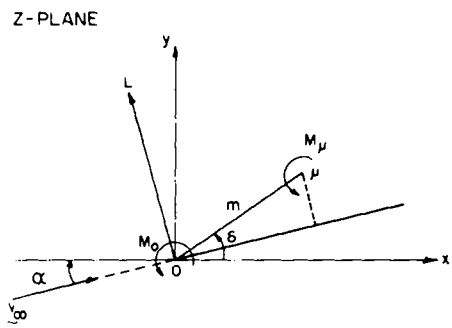

Figure 2. Nomenclature for force and moment on the aerofoil

If necessary, these integrals may be evaluated numerically, say, by the trapezoidal rule. Note that equations (18) evaluate the constants in a least squares sense. This is the only piece of numerical integration that may be needed, as was alluded to in the Introduction.

From equation (14) we now have

$$\psi(\phi)=\sum_{n=1}^{\infty}\hat{a}_n[\sin(n\phi)/\sin\phi]+\sum_{m=0}^{\infty}\hat{b}_m[\cos(m\phi)/\sin\phi]. \tag{19}$$

First iteration

Putting $\theta=\phi$, comparing equations (5) and (19) and noting that the y-co-ordinates at the aerofoil edges are zero, we have

$$\begin{aligned}
&(A_0)_1=(\chi_0)_1=\sum_{n=1,3}^{\infty}\hat{a}_n,\\
&(A_1)_1=2\sum_{n=2,4}^{\infty}\hat{a}_n,\\
&(A_p)_1=(A_{p-2})_1-2\hat{a}_{p-1},\quad p\geqslant 2,\\
&(B_1)_1=2\hat{b}_0,\\
&(B_2)_1=2\hat{b}_1,\\
&(B_p)_1=(B_{p-2})_1+2\hat{b}_{p-1},\quad p\geqslant 3.
\end{aligned} \tag{20}$$

The symbol $(\square)_1$ denotes values for the first iterate. Also, from equations (5) and (6) we obtain

$$\begin{aligned}
&\mathrm{d}\psi/\mathrm{d}\phi=\sum_{n=1}^{\infty}[-n(A_n)_1\sin(n\phi)+n(B_n)_1\cos(n\phi)],\\
&(\mathrm{d}\varepsilon/\mathrm{d}\phi)_1=\sum_{n=1}^{\infty}[n(B_n)_1\sin(n\phi)+n(A_n)_1\cos(n\phi)],\\
&(\theta)_1=\phi+(\varepsilon)_1,\qquad (\beta)_1=\sum_{n=1}^{\infty}(B_n)_1.
\end{aligned} \tag{21}$$

Second iteration

Let $(\square)_2$ denote values for the second iterate. Upon noting that $\psi(\theta)=\psi[\theta(\phi)]=\psi(\phi)$, we have

$$\begin{aligned}
(\chi_0)_2&=(1/2\pi)\int_0^{2\pi}\psi(\theta)\,\mathrm{d}\theta=(1/2\pi)\int_0^{2\pi}\psi(\phi)[1+(\mathrm{d}\varepsilon/\mathrm{d}\phi)_1]\,\mathrm{d}\phi\\
&=(\chi_0)_1+(1/2)\sum_{n=1}^{\infty}n[(A_n)_1^2+(B_n)_1^2],
\end{aligned} \tag{22}$$

$$\begin{aligned}
(A_p)_2&=(1/\pi)\int_0^{2\pi}\psi(\phi)\cos\{p[\phi+(\varepsilon)_1]\}[1+(\mathrm{d}\varepsilon/\mathrm{d}\phi)_1]\,\mathrm{d}\phi\\
&=(A_p)_1+\sum_{n=1}^{\infty}\sum_{m=1}^{\infty}[m(A_m)_1(A_n)_1I^{(2)}(m,n,p)\\
&\quad+m(B_m)_1(B_n)_1I^{(1)}(m,n,p)-p(A_m)_1(A_n)_1I^{(1)}(n,p,m)\\
&\quad+p(B_m)_1(B_n)_1I^{(1)}(m,p,n)]\\
&\quad+\text{third-order terms in semi-thickness and camber ratios,}
\end{aligned} \tag{23}$$

$$(B_p)_2 = (1/\pi)\int_0^{2\pi} \psi(\phi)\sin\{p[\phi+(\varepsilon)_1]\}[1+(\mathrm{d}\varepsilon/\mathrm{d}\phi)_1]\,\mathrm{d}\phi$$

$$= (B_p)_1 + \sum_{n=1}^{\infty}\sum_{m=1}^{\infty}[m(A_m)_1(B_n)_1 I^{(1)}(n,p,m) + m(B_m)_1(A_n)_1 I^{(1)}(m,p,n) + p(B_m)_1(A_n)_1 I^{(1)}(m,n,p) - p(A_m)_1(B_n)_1 I^{(2)}(m,n,p)]$$

$$+ \text{third-order terms in semi-thickness and camber ratios,} \tag{24}$$

where

$$I^{(1)}(i,j,k) = (1/\pi)\int_0^{2\pi} \sin(i\phi)\sin(j\phi)\cos(k\phi)\,\mathrm{d}\phi$$

$$= \begin{cases} 1 & \text{if } i=j,\ k=0, \\ -1/2 & \text{if } (i+j)=k,\ k\neq 0, \\ 1/2 & \text{if } |j-i|=k,\ k\neq 0, \\ 0 & \text{otherwise,} \end{cases} \tag{25}$$

$$I^{(2)}(i,j,k) = (1/\pi)\int_0^{2\pi} \cos(i\phi)\cos(j\phi)\cos(k\phi)\,\mathrm{d}\phi$$

$$= \begin{cases} 1 & \text{if } i=j,\ k=0, \\ 1/2 & \text{if } (i+j)=k \text{ or } |j-i|=k,\ k\neq 0, \\ 0 & \text{otherwise.} \end{cases} \tag{26}$$

In evaluating $(A_p)_2$ and $(B_p)_2$ we will neglect terms of third order in the semi-thickness and camber ratios since this is quite compatible with the fact that in calculating ψ, and hence ε, we have already neglected terms of the same order. The additional assumption made here is that $\mathrm{d}\varepsilon/\mathrm{d}\phi$ is also of the same order as ψ. On similar grounds, third and subsequent iterations need not be carried out as these again only bring about corrections of third or higher order in semi-thickness and camber ratios. For consistency, however, third and higher iterations would require that additional terms be included in the expression for ψ in equation (14).

The new values of θ, ε, $\mathrm{d}\varepsilon/\mathrm{d}\phi$ and β are now

$$(\theta)_2 = \phi + (\varepsilon)_2, \tag{27}$$

$$(\varepsilon)_2 = \sum_{n=1}^{\infty}\{(A_n)_2\sin[n(\theta)_1] - (B_n)_2\cos[n(\theta)_1]\}, \tag{28}$$

$$(\mathrm{d}\varepsilon/\mathrm{d}\phi)_2 = (\mathrm{d}\varepsilon/\mathrm{d}\theta\cdot\mathrm{d}\theta/\mathrm{d}\phi)_2 = (\mathrm{d}\varepsilon/\mathrm{d}\theta)_2[1+(\mathrm{d}\varepsilon/\mathrm{d}\phi)_2] = (\mathrm{d}\varepsilon/\mathrm{d}\theta)_2/[1-(\mathrm{d}\varepsilon/\mathrm{d}\theta)_2] \cong (\mathrm{d}\varepsilon/\mathrm{d}\theta)_2[1+(\mathrm{d}\varepsilon/\mathrm{d}\theta)_2], \tag{29}$$

where

$$(\mathrm{d}\varepsilon/\mathrm{d}\theta)_2 = \sum_{n=1}^{\infty}\{n(A_n)_2\cos[n(\theta)_1] + n(B_n)_2\sin[n(\theta)_1]\} \tag{30}$$

and

$$(\beta)_2 = -(\varepsilon(\phi = 0))_2. \tag{31}$$

With these new values we can now easily calculate $|W(z)|_C$ from equation (11) and lift and moment coefficients from Equations (12).

3.1. *Calculation at the aerofoil edges*

To avoid a spurious division by zero on a digital computer in calculating ψ at the aerofoil edges, equation (5) should be used instead of equation (14).

The Fourier representation of the aerofoil co-ordinates by equation (17) leads to the individual aerofoil edges being rounded or cusped. If the given aerofoil has rounded or cusped edges, it does not matter. However, if the edge is sharp (but not cusped), it will be rounded by the Fourier representation. Its immediate consequence is to move the critical point of the transformation associated with the edge from on the circle to inside the circle. Thus any singularity in the speed at a sharp (but not cusped) leading edge postulated by the exact conformal map will now disappear. At the trailing edge the change is more or less inconsequential since in any case the application of the Kutta condition at the edge would remove the singularity by forcing the edge to be a stagnation point.

We should, however, note in defence of the Fourier expansion for y that in practice the sharp leading edge aerofoil in the context of low-speed aerodynamics is of academic interest only. All aerofoils useful at low speed have a rounded leading edge, where the Fourier expansion of y is justified.

At a cusped trailing edge a computational problem arises on a digital computer, because $|W(z)|$ attains the form 0/0 owing to the point ζ_T in the ζ-plane (corresponding to the trailing edge point z_T in the z-plane) being a stagnation point and both ψ and ϕ being zero there. (At a cusped edge $dy/dx = dy/d\phi \cdot d\phi/dx = \sum_{n=1}^{\infty} [n\hat{a}_n \cos(n\phi) - n\hat{b}_n \sin(n\phi)]/\sin\phi = 0$, which means that at a cusped trailing edge, where $\phi = 0$, $dy/dx = \sum_{n=1}^{\infty} n\hat{a}_n = 0$. Since $[\sin(n\phi)/\sin\phi]_{\phi=0} = n$, it follows that $\psi = 0$ from equation (19) when one remembers that $\sum_{m=0}^{\infty} \hat{b}_m = 0$ due to $y = 0$ at the aerofoil trailing edge.) The problem may be avoided by calculating very close to the trailing edge, say at $(2x/c) = 0{\cdot}9999$, which for all practical purposes would be the value at the trailing edge. However, for the purist, the exact value at the trailing edge may be obtained as follows.

At the trailing edge (denoted by subscript T) we have

$$\phi_T = 0$$

and in the immediate vicinity of the trailing edge

$$\begin{aligned} \phi &= \phi_T + \Delta\phi = \Delta\phi, \\ \varepsilon &= \varepsilon_T + (d\varepsilon/d\phi)_T \Delta\phi = \varepsilon_T + \varepsilon'_T \Delta\phi, \\ \sin(\alpha+\beta) - \sin(\alpha-\theta) &= \sin(\alpha-\varepsilon_T) - \sin(\alpha - \Delta\phi - \varepsilon_T - \varepsilon'_T\Delta\phi) \\ &\cong \cos(\alpha-\varepsilon_T)(1+\varepsilon'_T)\Delta\phi. \end{aligned}$$

Thus

$$|W(z)|_T \cong \frac{V_\infty e^{\chi_0}(1+\varepsilon'_T)^2 \cos(\alpha-\varepsilon_T)}{\sqrt{\{[1+(\psi_T/\Delta\phi)^2][1+(d\psi/d\phi)_T^2]\}}}. \tag{32}$$

If ψ_T is not zero at the trailing edge, then $\psi_T/\Delta\phi$ will become infinite there and $|W(z)|$ will be zero (i.e. the trailing edge will be a stagnation point). On the other hand, ψ_T will be zero if the trailing

edge is cusped. Once again, in the vicinity of the trailing edge we may write

$$\psi = \psi_T + (d\psi/d\phi)_T(\Delta\phi) + (1/2)(d^2\psi/d\phi^2)_T(\Delta\phi)^2 + \ldots,$$

from which it follows that

$$\psi/\Delta\phi = \psi_T/\Delta\phi + (d\psi/d\phi)_T + (1/2)(d^2\psi/d\phi^2)_T(\Delta\phi) + \ldots$$
$$\cong (d\psi/d\phi)_T \quad \text{since } \psi_T = 0.$$

Therefore at the cusped trailing edge

$$|W(z)|_T = \frac{V_\infty e^{\chi_0}(1+\varepsilon_T')^2 \cos(\alpha-\varepsilon_T)}{1+(d\psi/d\phi)_T^2}. \tag{33}$$

This result differs from the one given by Pope[5] by the factor $\cos(\alpha-\varepsilon_T)$. This factor is put to unity there, which would be the case for $|\alpha-\varepsilon_T| \ll 1$.

4. ILLUSTRATIVE EXAMPLES

In this section we shall provide three examples which demonstrate the ease and accuracy with which the new calculation procedure may be used.

Example 1. *Flow past an ellipse*

Let an ellipse of thickness ratio τ be given by

$$y = \begin{cases} \pm\tau(1-x^2)^{1/2}, & -1 \leqslant x \leqslant 1, \\ \tau \sin\phi, & 0 \leqslant \phi \leqslant 2\pi. \end{cases}$$

Then $\hat{a}_1 = \tau$ and all other $\hat{a}_n$, $\hat{b}_n = 0$.

Thus for the first iteration we calculate

$$(\chi_0)_1 = \tau,$$
$$(A_p)_1 = 0, \quad p \geqslant 1,$$
$$(B_p)_1 = 0, \quad p \geqslant 0,$$
$$\psi(\phi) = \tau, \quad d\psi/d\phi = 0,$$
$$(\varepsilon(\phi))_1 = 0, \quad (\beta)_1 = 0, \quad (d\varepsilon/d\phi)_1 = 0,$$
$$(\theta)_1 = \phi;$$

and for the second iteration the values are

$$(\chi_0)_2 = (\chi_0)_1 = \tau$$
$$(A_p)_2 = 0, \quad p \geqslant 1,$$
$$(B_p)_2 = 0, \quad p \geqslant 0,$$
$$(\varepsilon(\theta))_2 = 0, \quad (\beta)_2 = 0, \quad (d\varepsilon/d\phi)_2 = 0,$$
$$(\theta)_2 = \phi.$$

Therefore at the end of both the first and second iterations we have

$$|W(z)|_C = \frac{V_\infty |\sin\alpha - \sin(\alpha-\phi)| e^\tau}{\sqrt{(\sinh^2\tau + \sin^2\phi)}}. \tag{34}$$

The exact solution for the ellipse is known to be

$$|W(z)|_{C(\text{exact})} = \frac{V_\infty(1+\tau)|\sin\alpha - \sin(\alpha-\phi)|}{\sqrt{(\tau^2\cos^2\phi + \sin^2\phi)}} \tag{35}$$

A comparison of the two solutions is shown in Table I for $\alpha = 0°$ and $\alpha = 10°$, with $\tau = 0{\cdot}18$; the comparison is seen to be excellent. It should be noted that the solution obtained for the ellipse in equation (34) is approximate because we chose the leading and trailing edges of the ellipse as critical points rather than its foci. In the latter case the results given by Theodorsen's method would have been exact at the end of the first iteration itself.

In this simple example the second iterated solution is identical to the first iterated solution. However, if a consistent third-order correction was attempted, it would be non-zero.

Example 2. Flow past an approximate symmetric Joukowski aerofoil

Let the aerofoil be given by

$$y = \begin{cases} \pm\tau_1(1-x)(1-x^2)^{1/2}, & -1 \leqslant x \leqslant 1, \\ \tau_1 \sin\phi - (1/2)\tau_1 \sin(2\phi), & 0 \leqslant \phi \leqslant 2\pi, \end{cases}$$

where the thickness ratio τ of the aerofoil is given by

$$\tau = \frac{3\sqrt{3}}{4}\tau_1.$$

Table I. Surface speed distribution on an 18% thick ellipse

Aerofoil co-ordinates		$\alpha = 0°$		$\alpha = 10°$	
x	y	$\lvert W(z)\rvert_C/V_\infty$ Theodorsen	$\lvert W(z)\rvert_C/V_\infty$ exact	$\lvert W(z)\rvert_C/V_\infty$ Theodorsen	$\lvert W(z)\rvert_C/V_\infty$ exact
−1·00000	0·00000	0·00000	0·00000	2·29735	2·27655
−0·95106	0·05562	1·03309	1·03219	2·14997	2·14810
−0·80902	0·10580	1·14421	1·14537	1·73829	1·74006
−0·58779	0·14562	1·16834	1·17004	1·54874	1·55099
−0·30902	0·17119	1·17611	1·17799	1·43933	1·44162
0·00000	0·18000	1·17808	1·18000	1·36474	1·36697
0·30902	0·17119	1·17611	1·17799	1·30662	1·30870
0·58779	0·14562	1·16834	1·17004	1·25396	1·25578
0·80902	0·10580	1·14421	1·14537	1·19138	1·19259
0·95106	0·05562	1·03309	1·03219	1·04581	1·04490
1·00000	0·00000	0·00000	0·00000	0·00000	0·00000
−1·00000	0·00000	0·00000	0·00000	2·29735	2·27655
−0·95106	−0·05562	1·03309	1·03219	0·11517	0·11507
−0·80902	−0·10580	1·14421	1·14537	0·51537	0·51589
−0·58779	−0·14562	1·16834	1·17004	0·75245	0·75354
−0·30902	−0·17119	1·17611	1·17799	0·87717	0·87857
0·00000	−0·18000	1·17808	1·18000	0·95563	0·95719
0·30902	−0·17119	1·17611	1·17799	1·00988	1·01149
0·58779	−0·14562	1·16834	1·17004	1·04723	1·04875
0·80902	−0·10580	1·14421	1·14537	1·06228	1·06335
0·95106	−0·05562	1·03309	1·03219	0·98899	0·98813
1·00000	0·00000	0·00000	0·00000	0·00000	0·00000

Then $\hat{a}_1=\tau_1$, $\hat{a}_2=-(1/2)\tau_1$ and all other $\hat{a}_n$, $\hat{b}_n=0$.

Thus for the first iteration we calculate

$$(\chi_0)_1=\tau_1,$$
$$(A_1)_1=-\tau_1,$$
$$(A_p)_1=0, \quad p\geqslant 2,$$
$$(B_p)_1=0, \quad p\geqslant 0,$$
$$\psi(\phi)=\tau_1(1-\cos\phi), \qquad \mathrm{d}\psi/\mathrm{d}\phi=\tau_1\sin\phi,$$
$$(\varepsilon(\phi))_1=-\tau_1\sin\phi, \qquad (\beta)_1=0, \qquad (\mathrm{d}\varepsilon/\mathrm{d}\phi)_1=-\tau_1\cos\phi,$$
$$(\theta)_1=\phi+(\varepsilon)_1;$$

and for the second iteration the values are

$$(\chi_0)_2=\tau_1+(1/2)\tau_1^2,$$
$$(A_1)_2=-\tau_1,$$
$$(A_p)_2=0, \quad p\geqslant 2,$$
$$(B_p)_2=0, \quad p\geqslant 0,$$
$$(\varepsilon(\theta))_2=-\tau_1\sin\theta_1, \qquad (\beta)_2=0,$$
$$(\mathrm{d}\varepsilon/\mathrm{d}\phi)_2=-\tau_1\cos\theta_1+\tau_1^2\cos^2\theta_1,$$
$$(\theta)_2=\phi+(\varepsilon)_1.$$

The speed on the aerofoil surface can be obtained by substituting the above values in equation (11).

An exact solution for this aerofoil is not available. Nevertheless, we can demonstrate the accuracy of the first iteration by comparing it with the second. This is done in Table II for a 12% thick aerofoil at $\alpha=0°$. It is seen that the difference between the two iterations is small enough for the first iteration to be sufficiently accurate for practical purposes.

Table II. Surface speed distribution on a 12% thick symmetric approximate Joukowski aerofoil; $\alpha=0°$

Aerofoil co-ordinates		$\lvert W(z)\rvert_C/V_\infty$	
x	y	First iteration	Second iteration
−1·00000	0·00000	0·00000	0·00000
−0·95106	0·03133	1·10175	1·10805
−0·80902	0·05525	1·12833	1·13250
−0·58779	0·06675	1·11093	1·11231
−0·30902	0·06469	1·08203	1·08128
0·00000	0·05196	1·04908	1·04767
0·30902	0·03415	1·01656	1·01611
0·58779	0·01733	0·98786	0·98952
0·80902	0·00583	0·96559	0·96967
0·95106	0·00079	0·95152	0·95750
1·00000	0·00000	0·94671	0·95340

Example 3. Flow past a symmetric Karman–Trefftz biconvex aerofoil

Let the aerofoil be given by

$$y = \pm[y_0 + (R_0^2 - x^2)^{1/2}], \quad -1 \leqslant x \leqslant +1.$$

This biconvex aerofoil is composed of two circular arcs of radius R_0, and the centres of the circles of which the arcs are a part are located at $(0, \pm y_0)$. If the thickness ratio of the aerofoil is τ, then

$$R_0 = (1 - y_0^2)^{1/2}, \qquad y_0 = -(1 - \tau^2)/2\tau.$$

A sufficiently accurate Fourier series for the aerofoil with $\tau = 0{\cdot}20$ shows that

$$\begin{aligned}
\hat{a}_1 &= \ 0{\cdot}17111578, & \hat{a}_2 &= 0{\cdot}0,\\
\hat{a}_3 &= -0{\cdot}32964876 \times 10^{-1}, & \hat{a}_4 &= 0{\cdot}0,\\
\hat{a}_5 &= -0{\cdot}52849144 \times 10^{-2}, & \hat{a}_6 &= 0{\cdot}0,\\
\hat{a}_7 &= -0{\cdot}17140302 \times 10^{-2}, & \hat{a}_8 &= 0{\cdot}0,\\
\hat{a}_9 &= -0{\cdot}77171970 \times 10^{-3}, & \hat{a}_{10} &= 0{\cdot}0,\\
\hat{a}_{11} &= -0{\cdot}41386187 \times 10^{-3}, & \hat{a}_{12} &= 0{\cdot}0,\\
\hat{a}_{13} &= -0{\cdot}24762734 \times 10^{-3}, & \hat{a}_{14} &= 0{\cdot}0,\\
\hat{a}_{15} &= -0{\cdot}15978169 \times 10^{-3}, & \hat{a}_{16} &= 0{\cdot}0.
\end{aligned}$$

The remaining $\hat{a}_n$ are approximated to zero. All the $\hat{b}_n$ are of course zero.

For this case the speed on the aerofoil surface at $\alpha = 0°$ is tabulated in Table III which also contains the exact solution obtained by means of the Karman–Trefftz mapping. It is seen that even for this 20% thick aerofoil the first iteration itself agrees very well with the exact solution.

5. DISCUSSION AND CONCLUSIONS

The new method is easy to use and program on a digital computer. The excellent accuracy of the method is testified to by the examples shown in Section 4. Although the maximum thickness ratio there was chosen to be 20%, equally good results were obtained even for 30% thickness ratios for all the examples. This should not come as a surprise since the semi-thickness ratio is still only 15%

Table III. Surface speed distribution on a 20% thick Karman–Trefftz biconvex aerofoil. $\alpha = 0°$

Aerofoil co-ordinates			$\lvert W(z)\rvert_C / V_\infty$		
x	y (Fourier representation)	y (exact)	First iteration	Second iteration	Exact Karman–Trefftz
−1·00000	0·00000	0·00000	0·00000	0·00000	0·00000
−0·92860	0·02865	0·02852	0·82508	0·84354	0·84230
−0·76704	0·08428	0·08428	1·02275	1·02702	1·03121
−0·54464	0·14224	0·14232	1·15081	1·15174	1·15692
−0·28232	0·18462	0·18463	1·22715	1·23226	1·23243
0·00000	0·20006	0·20000	1·25296	1·26117	1·25780
0·28232	0·18462	0·18463	1·22715	1·23226	1·23243
0·54464	0·14224	0·14232	1·15081	1·15174	1·15692
0·76704	0·08428	0·08428	1·02275	1·02702	1·03121
0·92860	0·02865	0·02852	0·82508	0·84354	0·84230
1·00000	0·00000	0·00000	0·00000	0·00000	0·00000

and the neglected third-order terms would generally affect the third significant figure in the calculations. One can show this by roughly calculating the third-order terms.

Once the $\alpha = 0°$ case has been calculated, the speed on the aerofoil surface at any other α can be easily obtained by the simple relation

$$|W(z)|_C = \left| \frac{\sin(\alpha+\beta) - \sin(\alpha-\theta)}{\sin\beta + \sin\theta} \right| |W(z)|_{C \text{ at } \alpha = 0°}. \tag{36}$$

The Fourier representation for y was chosen because it is dictated by the Fourier representation of ψ. Therefore our discussion in Section 3.1 regarding the aerofoil edges would be equally valid irrespective of how one implemented Theodorsen's method.

The analytical form of the present results should be an advantage in solving the inverse problem; that is, designing an aerofoil to sustain a given pressure distribution. This aspect is now being looked into by the author.

Finally, we remark that the present method of a two-iteration solution is more accurate than Goldstein's third approximation[6] which has the accuracy of the first iteration of the present method.

REFERENCES

1. Th. Theodorsen, 'Theory of wing sections of arbitrary shape', *NACA Report No. 411*, 1931.
2. Th. Theodorsen and I. E. Garrick, 'General potential theory of arbitrary wing sections', *NACA Report No. 452*, 1933.
3. I. H. Abbott and A. E. von Doenhoff, *Theory of Wing Sections*, Dover Publications Inc., New York, 1959, ch. 3.
4. A. Robinson and J. A. Laurmann, *Wing Theory*, Cambridge University Press, 1956, ch. 2.
5. A. Pope, *Basic Wing and Airfoil Theory*, McGraw-Hill Book Co., Inc., New York, 1951, ch. 8.
6. S. Goldstein, 'A theory of airfoils of small thickness, parts 1–6', *Current Papers Nos 68–73*, ARC, London, 1952.